The International Journal of Advanced Manufacturing Technology
https://doi.org/10.1007/s00170-021-08031-0

ORIGINAL ARTICLE

Oxidation and wear behavior of high-speed steel and semi-high-speed steel used in hot strip mill

Fabienne Delaunois[1] · **Victor Ioan Stanciu**[1] · **Alexandre Megret**[1] · **Mario Sinnaeve**[2]

Received: 20 April 2021 / Accepted: 8 September 2021

Abstract

Depending on various properties such as hardness, roughness, friction coefficient, wear resistance, and oxidation behavior, different grades of steel can be used in hot strip mills. In this paper, two grades were investigated: one grade of semi-high-speed steel and one grade of high-speed steel. They differ in their chemical composition, principally the carbon and the chromium content, and the presence or not of other alloying elements such as vanadium, niobium, and tungsten. Their oxidation behavior was studied at 576 °C and 600 °C, temperatures reached in the F1 finishing stand and the roughing stand, respectively, by high-temperature oxidation tests in a wet atmosphere. The sliding wear resistance was followed by pin-on-disc experiments. The evolution of the microstructure was observed by optical and scanning electron microscopies. The oxides formed on the surface of the samples were analyzed by XRD and EDS. The thickness of the oxide layers and the mass gain were measured from oxidation tests. The results showed that for both grades, the surface roughness R_a after oxidation tests is high enough to prevent slipping. The low friction coefficient will increase the wear resistance of the roll. The hardness of the steel grades decreases but remains high enough to ensure wear resistance. Consequently, those grades can be used in the roughing stand or the F1 finishing stand of hot rolling mills.

Keywords Hot strip mill · High-speed steel · Semi-high-speed steel · Oxidation · Pin-on-disc

1 Introduction

High-speed steel (HSS) and semi-high-speed steel (semi-HSS) are used to manufacture the outer part of work rolls for hot roll mills.

The typical microstructure of HSS grade is made of a tempered martensite matrix which contains three primary eutectic carbides (about 9–15 vol.% fraction) due to the presence of Cr, Mo, and V [1]: MC, M_2C, and M_7C_3 types, and fine and homogeneous MC secondary hardening precipitates in the matrix. The main primary carbide is MC-type (more particularly VC carbides) generally distributed within the microstructure; the two other eutectic carbides found, M_2C-type rich in Mo (and in a lesser extent rich in W) and M_7C_3-type rich in Cr, generally precipitate together [1–11]. For specific HSS grades, M_6C carbides rich in Mo (and to a lesser extent rich in W) can be found along grain boundaries, mixed with M_7C_3-type [1, 11–13]. In the tempered matrix, fine spheroidal carbides $M_{23}C_6$-type are also found [1].

The semi-HSS grade mainly contains C, Cr, W, Mo, and MC-carbide forming elements such as V, Ti, Nb, and Ta. It is characterized by a tempered martensite matrix with embedded carbides such as M_7C_3, M_6C, and MC-types [14–17].

For the finishing stands, the main requirements for the choice of the good steel grade are the following: (i) high wear resistance, (ii) low friction coefficient, (iii) good resistance to rolling incidents, and (iv) good oxidation and thermal behavior [5]. For roughing stand, they are (i) high hot properties, (ii) good biting behavior (high coefficient of friction), (iii) high wear resistance, (iv) good surface condition (homogeneous and no too rough), (v) high roughness

✉ Fabienne Delaunois
fabienne.delaunois@umons.ac.be

Victor Ioan Stanciu
victorioan.stanciu@umons.ac.be

Alexandre Megret
alexandre.megret@umons.ac.be

Mario Sinnaeve
mario.sinnaeve@mkb.be

[1] Service de Métallurgie, Faculté Polytechnique, Université de Mons, rue de l'Epargne, 56, 7000 Mons, Belgium

[2] Marichal Ketin, Rue Ernest Solvay 372, 4000 Liege, Belgium

Published online: 06 November 2021

to prevent slipping, (vi) good resistance to the incident, and (vii) high hardness [16–18].

Friction and wear represent two key aspects of the tribological behavior of materials and result from exposure of the material to a particular set of conditions. When hard particles are present, the wear process involves abrasion (by sliding or rolling particles) [19, 20]. When the carbon content of the steel is high, carbides are formed during tempering treatment [21]. Those carbide inclusions provide additional abrasive wear resistance. Some alloying elements are also useful for this purpose, such as chromium, molybdenum, and niobium, and/or vanadium, since the obtained carbides are extremely hard (about 1300–1400 HV for M_7C_3 chromium-rich carbide, about 1500 HV for M_2C molybdenum-rich carbide, and about 2400 HV for MC niobium and/or vanadium-rich carbide) [1, 20].

The wear phenomena of work rolls are complex processes of sliding wear, where thermal fatigue combines with abrasion, adhesion, and oxidation/corrosion [22–25]. For sliding wear observed in hot strip mill, abrasion should not be a dominant mechanism, even if wear debris coming from oxidized surface films can result in abrasion [22]. The calculations of the coefficient of friction and the amount of wear in sliding contact are of great practical interest [22]. Consequently, the roll performance and the surface quality of rolled products are directly affected by the oxidation of the roll surface. It is thus important to understand the oxidation behavior of the steel grades and to study their resistance to wear. F.H.Stoot [26] has shown that oxidation can be beneficial by reducing wear during the sliding of metals, particularly by preventing metal–metal contact. Moreover, the oxidation behavior of a work roll is strongly influenced by temperature, time, environmental conditions, chemical composition (i.e., chromium content), distribution, and volume fraction of carbides [1, 9].

As the rolls are cooled with water during the rolling process, it is interesting to study the oxidation behavior of the steel in a wet atmosphere. The humid atmosphere leads to more heavy oxidation than the dry one at the same temperature, due to the presence of water vapor that prevents the formation of the protective chromium oxide layer which is naturally forming in dry air [4, 22, 27–29]. Garza-Montes-de-Oca and Rainforth [9] have reported that for rolling-sliding wear experiments between 400 and 600 °C, the specific wear rate under water lubricated conditions is very lower than under dry conditions. They have also proved that the wear rate is essentially temperature independent and that the wear mechanism is principally oxidational at all temperatures. They have shown that the presence of water and water vapor increased the degree of oxidation on the surface of HSS work rolls, with the formation of a spinel M_3O_4, as well as Fe_2O_3, which is not present for the dry conditions.

According to the position of the work roll in the rolling mill, the maximum temperature of the roll surface varies. Deng et al. [4, 30] showed that this one varies from 580 to 650 °C at the stand F1, to quickly decrease from stand F1 to F4, and to reach about 340 °C. Belzunce et al. [1] have shown that just after the establishment of contact between the work roll and the strip, the roll surface temperature rises very quickly to tend to level off at a value that is dependent on the position of the stand. In the initial finishing stands, due to the high temperature of the strip, the highest contact time between roll and strip, and the lowest strip speed, the temperature peak is very high, near 500–550 °C. S. Serajzadeh [31] has predicted temperature variations within the work rolls. He has shown that the temperature distribution depended on the rolling parameters, such as interstand time, length of the slab, reduction in each pass, rolling speed, and interface heat transfer coefficient. In roughing mills, the temperature of the roll surface is known to be heated up to more than 600 °C when it is in contact with the hot slab [14]. Belzunce et al. [1] have shown that peak roll temperatures are about 75 °C higher in the roughening stands compared to the initial finishing stands, to reach about 600 °C. Weidlich et al. [32] have proved that operational parameters of a hot rolling mill impacted the degradation process of a roll surface by thermal fatigue by studying roll surface temperature and heat-penetration depth.

The formation of oxidation products of iron, wüstite (FeO), magnetite (Fe_3O_4), and hematite (Fe_2O_3) depends on the temperature [33]. The scale formed on the iron strip surface is thus composed of three layers: the outside layer Fe_2O_3 (average hardness at room temperature of 1000 HV), a middle layer of Fe_3O_4 (about 450 HV), and an inner layer FeO (about 350 HV). Moreover, the oxide thickness depends on the strip temperature. In roughing stands, with a strip temperature of about 1150–1250 °C, the scale is composed of a large amount of abrasive Fe_2O_3 scale, while in the last finishing stands, the soft FeO scale is predominant [1]. Magnée et al. [25] have shown that in the case of sliding wear, the oxides will play an abrasive or lubricant role according to their nature. It is generally assumed that Fe_3O_4 results in lower wear intensity than Fe_2O_3 oxide films [22]. However, as magnetite and hematite layers have high hardness, they also act as abrasive layers. On the other hand, wüstite presents a softer, porous layer that plays a lubricating role between the surfaces in contact. In HSS steels, wüstite is not detected in XRD patterns [8]. In low alloy steels, above 570 °C, the formation of wüstite is prevented if the chromium content in the steel is sufficiently high [33]. The presence of chromium favors the wüstite transformation into magnetite or chromium-rich spinel structure.

Combined with good coverage of the rubbing surfaces, a greater oxide film thickness, obtained with an increase

of the contact temperature, can provide a greater protective capability to sliding wear [22].

This paper presents a comparison of the oxidation behavior of HSS and semi-HSS grades at 576 °C and 600 °C, temperatures reached in the F1 finishing stand, and the roughing stand, respectively. After oxidation tests, the wear resistance of both grades was compared to determine if those grades can be used in the roughing stand or the F1 finishing stand of hot rolling mills.

2 Materials and methods

2.1 Materials and sample preparation

The chemical composition of the HSS and semi-HSS samples investigated in this work is presented in Table 1.

They come from commercial centrifugal hot work rolls. They were heat-treated in Marichal Ketin's furnaces following the industrial optimized process for each grade (austenization followed by double-tempering).

A detailed description of the specimens cutting is given in [12].

Specimens for microstructural observation were ground with abrasive papers (up to P4000 grade), mirror polished using a 1-µm diamond polishing paste to allow microscopic observations, and then etched with 4 vol.% Nital. Some specimens were also etched with Murakami color etchant.

Specimens for oxidation experiments were $22 \times 22 \times 3.5$ mm of dimensions. All their sides were ground and polished with abrasive paper (P500 grade) to obtain the same level of roughness ($R_a = 0.13 \pm 0.02$ µm). Care was taken to reproduce the same grinding and polishing procedure for all the specimens.

2.2 Isothermal oxidation experiment in a humid atmosphere

The gravimetric mean used in this study is home-made and described in [12].

The temperature test was chosen to simulate thermal conditions encountered by the work rolls in hot strip mills, 600 °C ± 1 °C, and 576 °C ± 1 °C. Once this temperature was reached (after approximately 10 min), the water vapor was introduced at the bottom of the reactor and the oxidation kinetics was observed for 65 min. The mass change was precisely measured before and after the tests and continuously recorded during the high-temperature exposure, with an electronic balance Mettler AE 260 (accuracy of measurements of 0.1 mg). Three experiments were performed for each grade.

2.3 Analytical methods

Digital optical microscopy (Hirox 8700 3D) and scanning electron microscopy SEM coupled with energy dispersive X-rays spectrometry (EDS) (Hitachi 8020) were used to characterize the surface morphology and the microstructure of the samples, as well as the corrosion products formed on the surface of the specimens during the oxidation process. The thickness of the oxide layers was measured using digital optical microscopy on the cross section of oxidized samples. The structure of the oxide phases was identified by X-ray diffraction (Philips X-rays apparatus applying Co K_α (1.7902 Å)).

After the oxidation test, a surface profilometer (Nano-Jura High Precision Surface Metrology System-NJHP 505, confocal gauge head of 1 mm, length of 18 mm, speed of 500 µm s^{-1}) was used to characterize and quantify the surface roughness of all samples.

The macrohardness was measured using an Emco M4U-02 hardness tester with a Vickers indenter using a load of 30 kgf with a minimum of five measurements per test. Measurements were performed on cross-sections to avoid the influence of the fragile oxide layer.

To determine the interactions between the development of friction and the nature of oxides found on the sample's surface, the sliding wear resistance of the external oxide scale was investigated by a conventional pin-on-disk tribometer at room temperature, using dedicated software (InstrumX version 2.5A, CSM Instruments). The disks were samples of the studied grades previously submitted to oxidation tests, and the counterparts were 6-mm diameter alumina balls. The sliding speed and sliding distance were 5 cm/s and 10 m, respectively. Wear tests were carried out under normal loads of 0.25 N at room temperature. Three measurements were performed for all grades.

Table 1 Chemical composition of the studied ferrous alloys grades (wt%)

	C	Cr	Ni	Mo	V	Nb
HSS	1.3–1.6	4.0–6.0	1.0–1.5	2.0–4.0	4.0–5.0	-
Semi-HSS	0.9–1.3	7.5–10.0	0.45–1.1	2.5–4.5	0.2–1.6	0.8–2.0
	W	Si	Mn	Weq (W + 2 mo)	MC-Carbide forming (V + Ti + Nb)	
HSS	1.5–2.5	0.1–1.0	0.5–1.0	8.0–10.0	4.0–5.0	
Semi-HSS	-	0.6–1.2	0.5–1.0	5.0–9.0	1.0–3.6	

3 Results

3.1 XRD analysis of the oxide layers after oxidation tests at 576 °C and 600 °C

Whatever the oxidation temperature and the grade studied, after oxidation tests, an outer ferrous oxide layer is observed. In Fig. 1, XRD analysis shows the presence of Fe_2O_3 and Fe_3O_4 peaks as the most abundant species found in the oxidation layer. A spinel $FeCr_2O_4$, produced by internal oxidation, is also found. No FeO is detected in the samples. Traces of CrO are also found.

3.2 Microstructure of the specimens after oxidation tests

The microstructure of the specimens after oxidation tests at 576 °C is presented in Fig. 2 after Nital etching and Murakami coloring. Figures 3 and 4 present the SEM micrographs and EDS mappings of semi-HSS and HSS grades, respectively.

For both grades, no continuous carbide network was found. For all specimens, Fig. 2 shows that the oxidation scale is composed of two layers, a porous outer one (lighter) with many defects and a denser inner one (darker), with a clear interface between the two layers that is the initial metal surface. The tempered martensite matrix is homogeneously oxidized. For HSS grade, the inner oxide layer contains many primary carbides that are not affected by the oxidation progress (Fig. 2c).

From Figs. 2 and 3, the microstructure of the semi-HSS grade contains a tempered martensite matrix with $M_{23}C_6$ carbides and eutectic carbides of M_7C_3-type (Fig. 2a — brown — lamellae) containing Cr, Mo, Nb, and V (Fig. 3) and M_2C-MC-type (Fig. 2a — dark pink — acicular) containing Nb, Cr, and V (Fig. 3) at the grain boundaries. From Figs. 2 and 4, the microstructure of the HSS grade is composed of MC-type (Fig. 2d — light rose — globular morphology) containing V, Mo, W, and Cr (Fig. 4) and M_2C-type (Fig. 2d — dark — cluster of rod-like particles) carbides containing Mo, Cr, and V (Fig. 4), embedded in a tempered martensite matrix containing $M_{23}C_6$ carbides. No affected MC-type carbides are found in the inner oxide layer.

The amount of total carbides in semi-HSS grade is lower than in HSS grade.

The test temperature does not influence the microstructure of the specimens, as illustrated by the oxidations tests at 600 °C (Fig. 5).

3.3 SEM and EDS analysis of the oxide layers

The SEM microstructure and interpretation of chemical analysis from the EDS analysis are presented in Fig. 6.

After the oxidation test at 576 °C, both grades (Fig. 6a and b) present an outer oxide layer with many cracks that can reach the non-oxidized matrix through the inner oxide layer. The oxidation progression seems to be uniform from the surface to the substrate. The oxide scale (point 2 in Fig. 6a and b) grows homogeneously through the tempered martensite matrix (point 3 in Fig. 6a and b). This outer oxide layer is composed of iron oxide (point 1 in Fig. 6a and b). Figure 6a shows that for the semi-HSS grade, the M_7C_3 and MC carbides present in the inner oxide layer also show little oxidation (points 4 and 5 in Fig. 6a). For the HSS grade (Fig. 6b), the oxidation also progresses

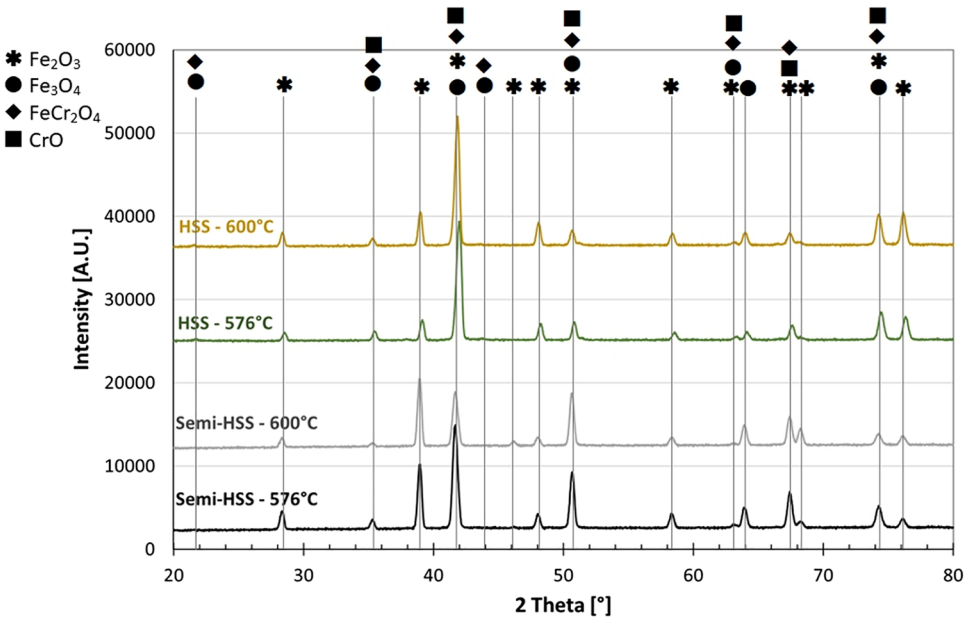

Fig. 1 XRD patterns of top samples after oxidation tests at 576 °C and 600 °C

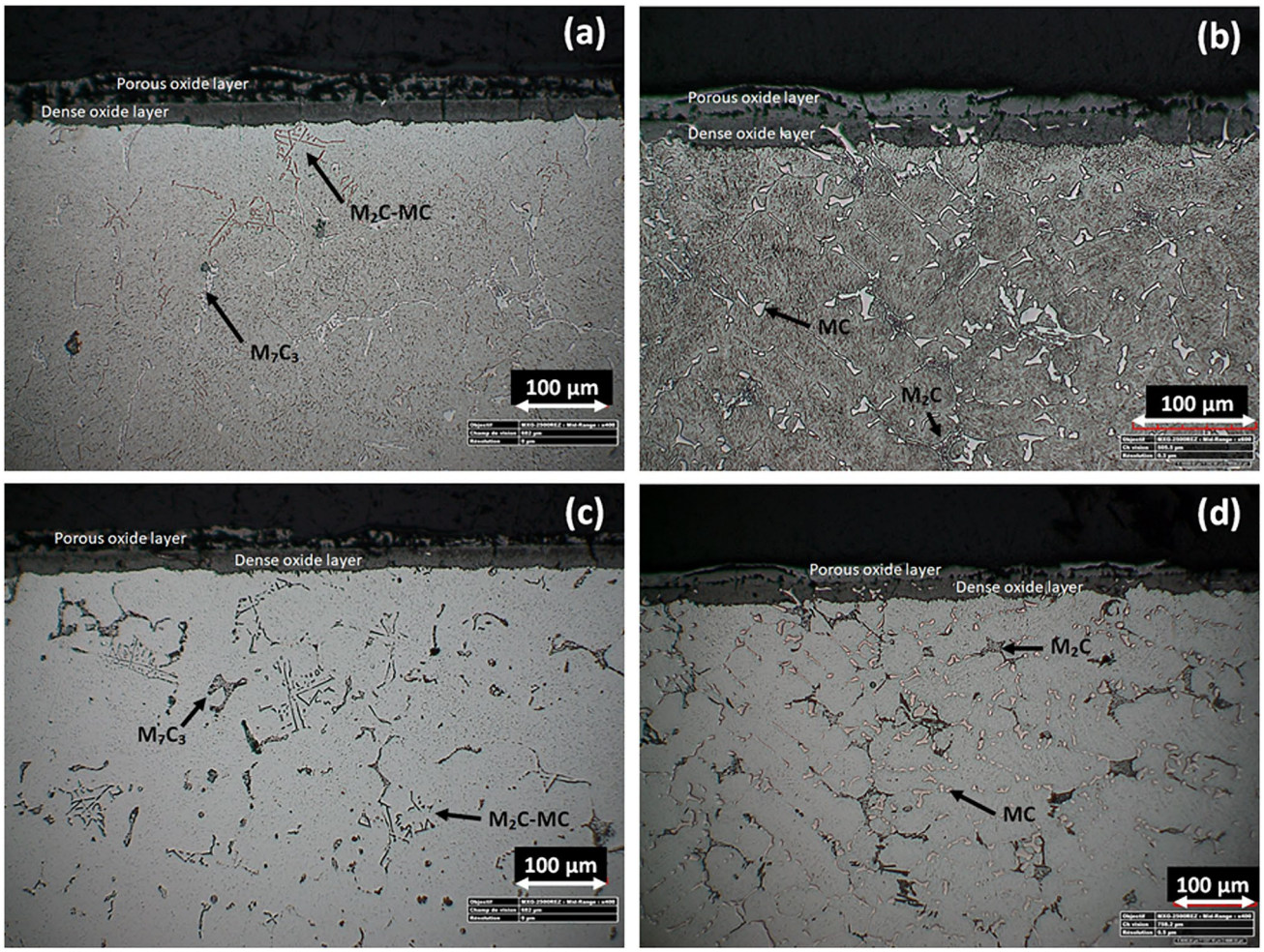

Fig. 2 Microstructure of the specimens after oxidation at 576 °C — optical microscopy: after Nital etching: **a** semi-HSS 1 grade; **b** HSS grade; after Murakami coloring: **c** semi-HSS grade; **d** HSS grade

inside the sample by penetration through the M_2C carbides (point 4 in Fig. 6b), but contrary to the semi-HSS grade, MC carbides are not affected by the oxidation progress (point 5 in Fig. 6b).

After the oxidation test at 600 °C, Fig. 6c shows that semi-HSS grade presents a thick outer oxide layer with a longitudinal crack near the surface of the substrate. The oxidation progression is uniform from the surface to the substrate through the tempered martensite matrix. The M_7C_3 carbides (point 4 in Fig. 6c) present in the inner oxide layer show oxidation, while MC carbides (point 5 in Fig. 6c) seem not to be affected. Figure 6d shows that the HSS grade has an outer iron oxide layer containing cracks. This layer seems to better adhere to the substrate comparing to the semi-HSS sample. Contrary to the semi-HSS grade, MC carbides (point 4 in Fig. 6d) are not affected by oxidation progress. The oxidation progresses inside the sample by penetration through the M_2C carbides (point 5 in Fig. 6d).

3.4 Macrohardness measurements

From Fig. 7, before oxidation tests, the Vickers hardness of both grades is of the same order of amplitude, about 680 HV_{30}. After oxidation tests, the hardness of both grades decreases whatever the temperature. For the HSS grade, the hardness after heat treatment at 576 °C (573 ± 12 HV_{30}) is a little bit higher than after oxidation at 600 °C (548 ± 16 HV_{30}). The semi-HSS grade suffers from the most important reduction of hardness (about 25%). For this grade, the hardness after heat treatment at 600 °C (522 ± 19 HV_{30}) gives a higher mean value than after oxidation at 576 °C (499 ± 10 HV_{30}), but with a higher standard deviation. This observation is therefore not scientifically relevant since the mean values obtained for both temperatures cannot be distinguished from one to another.

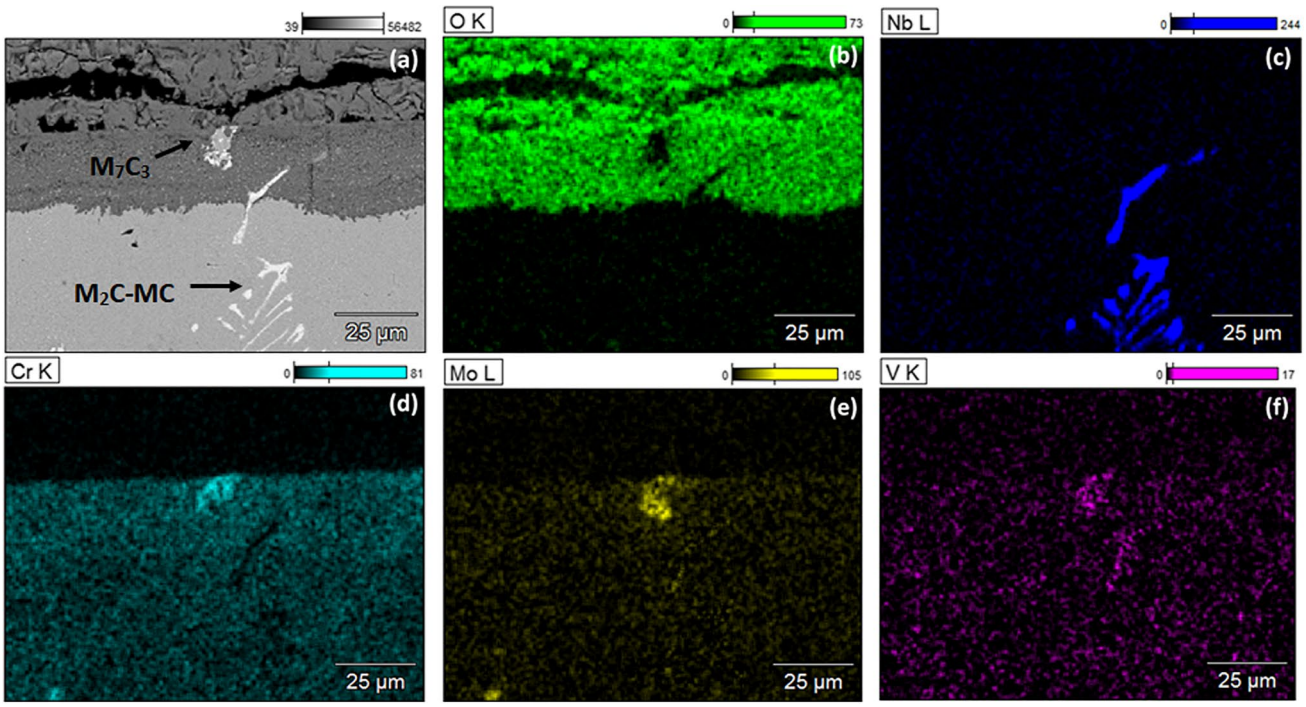

Fig. 3 SEM microstructure (**a**) and EDS mapping for O (**b**), Nb (**c**), Cr (**d**), Mo (**e**), and V (**f**) for semi-HSS grade after oxidation test at 576 °C

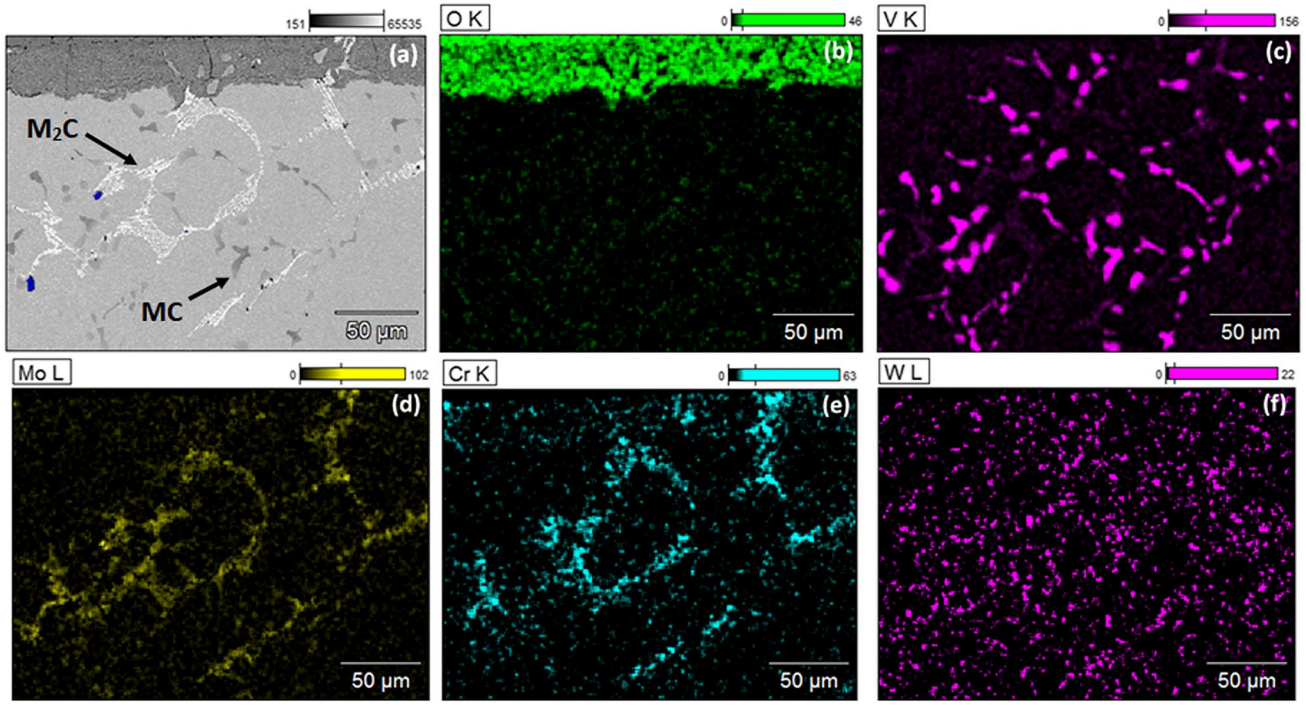

Fig. 4 SEM microstructure (**a**) and EDS mapping for O (**b**), V (**c**), Mo (**d**), Cr (**e**), and W (**f**) for HSS grade after oxidation test at 576 °C

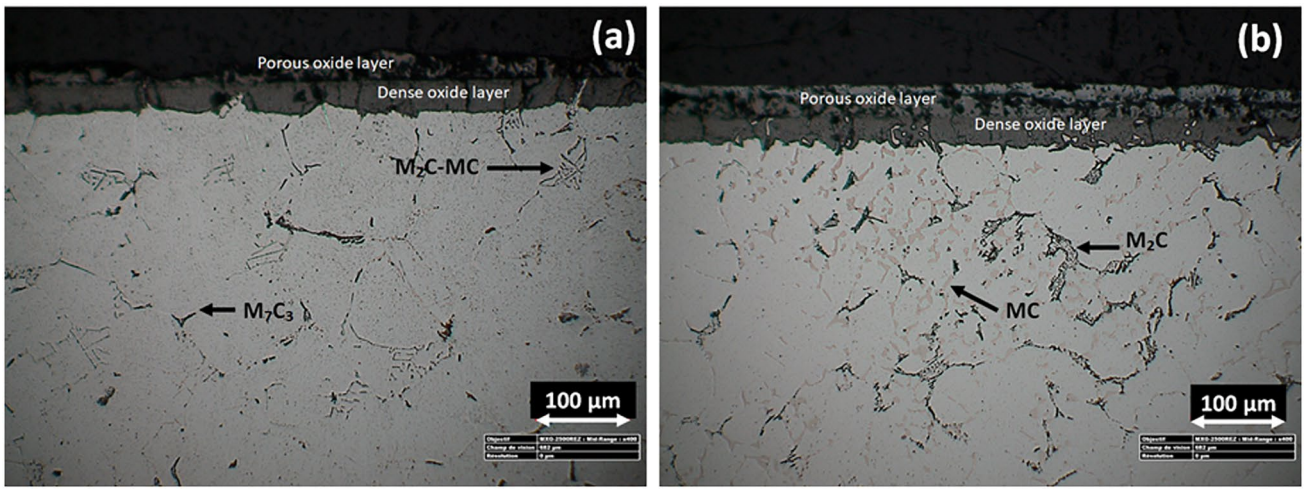

Fig. 5 Microstructure of the specimens after oxidation at 600 °C — optical microscopy: after Murakami coloring: **a** semi-HSS grade; **b** HSS grade

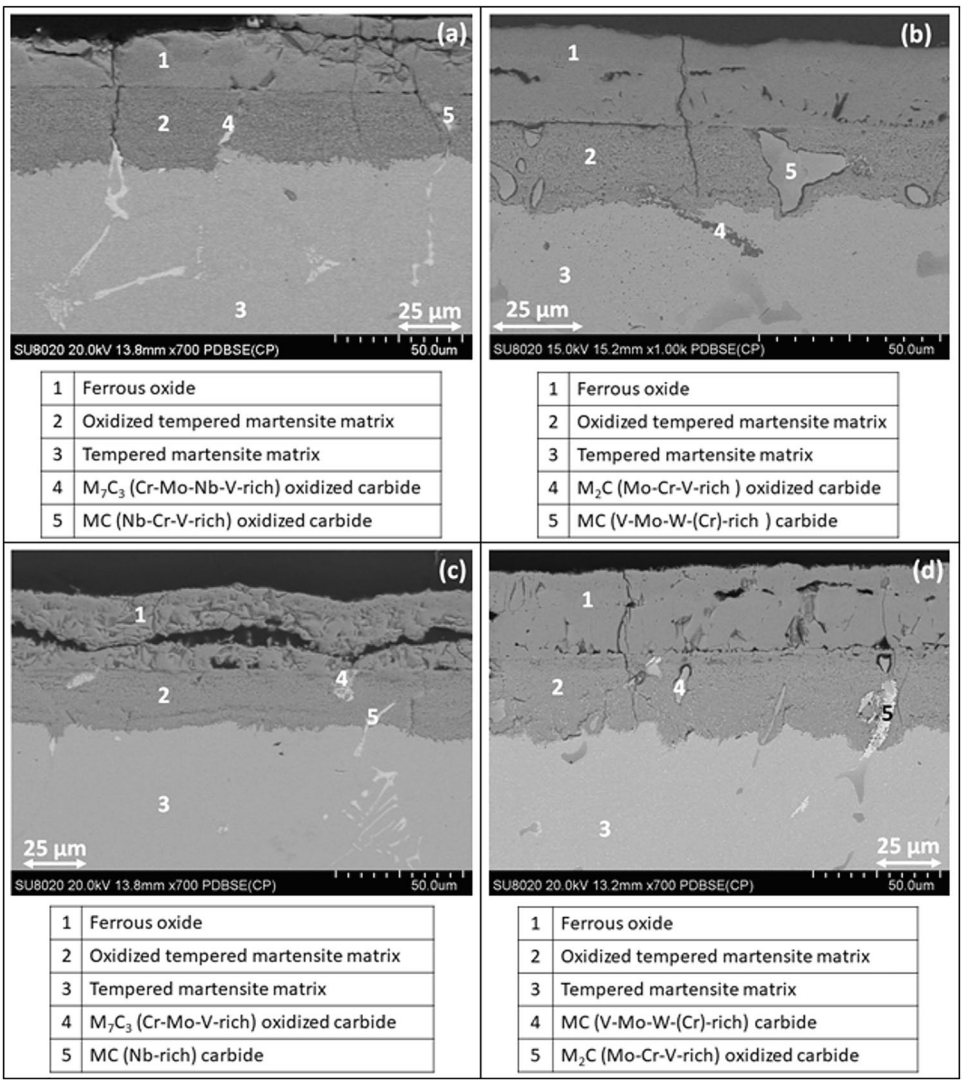

Fig. 6 SEM microstructures after oxidation test at 576 °C for semi-HSS grade (**a**) and HSS grade (**b**); after oxidation test at 600 °C for semi-HSS grade (**c**) and HSS grade (**d**)

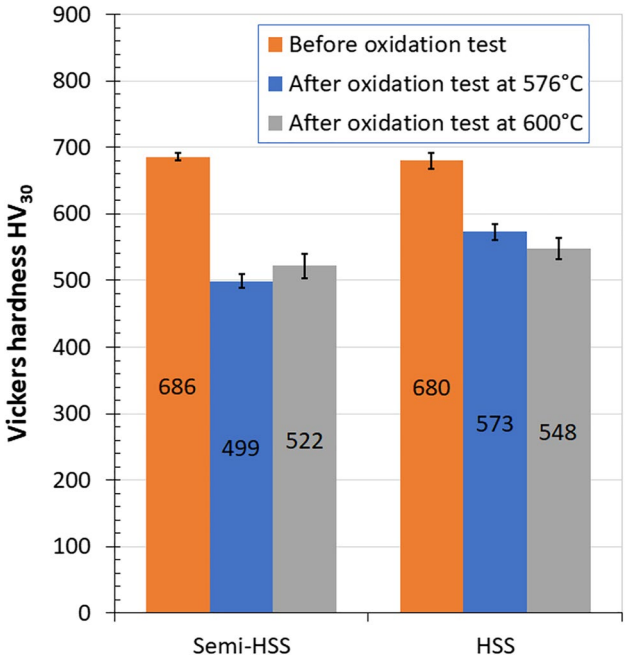

Fig. 7 Vickers macrohardness HV_{30} before and after oxidation tests at 576 °C and 600 °C

3.5 Thickness and roughness of the oxide layers

Table 2 shows the average total, outer and inner oxide layer thicknesses for each specimen. The total oxide layer thickness increases from 576 to 600 °C for both specimens. However, the inner oxide layer thickness is in the same order of magnitude that the outer one for all samples and both temperatures of oxidation test considering the standard deviation.

Surface roughness is widely used for describing surface quality, despite its limited evidence [22]. The initial R_a for all the samples is 0.13 ± 0.02 µm. Table 3 shows a great increase in the R_a after the oxidation test. This can be linked to the formation of the scale on the surface of the specimen. R_a increases with the temperature of the oxidation test, except for the HSS grade for which it remains constant. For the semi-HSS grade, R_z and R_p greatly increase with the temperature of the oxidation test, which means that the scale profile contains higher peaks and bigger valleys after oxidation at 600 °C.

All the results confirm the microscopic observations.

3.6 Oxidation kinetic curves and mass changes

From Table 4, as expected, the higher is the oxidation temperature, the higher is the mass gain. For both oxidation temperatures, the semi-HSS grade exhibits a higher mass gain than the HSS grade, and the semi-HSS grade shows the highest mass gain after the oxidation test at 600 °C.

The oxidation is temperature-dependent as the general equation of the oxide layer growth can be expressed as Eq. 1 [34],

$$e_0 = k_p \times t^n \tag{1}$$

where e_0 is the thickness of the scale at time t and k_p is the growth coefficient which depends on the type of oxide

Table 2 Average total, outer, and inner oxide layer thickness (µm) for the various samples after oxidation tests at 576 °C and 600 °C in a humid atmosphere

Temperature of oxidation test (°C)	Oxide layer thickness (µm)					
	Semi-HSS			HSS		
	Outer	Inner	Total	Outer	Inner	Total
576	24.4 ± 5.9	25.9 ± 1.7	50.8 ± 7.6	26 ± 3.2	23.3 ± 1.6	49 ± 6.7
600	35.9 ± 5.4	35.1 ± 2.2	70.8 ± 6.7	30.3 ± 7.1	29.7 ± 5.4	60 ± 12.6

Table 3 Surface roughness (µm) of the oxidized samples after oxidation tests at 576 °C and 600 °C

	Semi-HSS		HSS	
Temperature of oxidation test (°C)	576	600	576	600
R_a (µm)	2.78 ± 0.18	4.65 ± 0.23	2.52 ± 0.24	2.51 ± 0.30
R_z (µm)	20.48 ± 1.77	30.83 ± 1.13	18.89 ± 2.39	18.79 ± 1.82
R_p (µm)	8.33 ± 0.64	13.07 ± 0.58	8.54 ± 1.25	9.49 ± 1.23

Table 4 Mass gain (mg/mm^2) of the various samples after oxidation tests in a wet atmosphere at 576 °C and 600 °C

	Temperature of oxidation test (°C)			
	576		600	
Grade	Semi-HSS	HSS	Semi-HSS	HSS
Masse gain (mg/mm^2)	0.066 ± 0.002	0.056 ± 0.001	0.080 ± 0.002	0.061 ± 0.005

and temperature and n the type of oxidation mechanism. If $n = 1$, oxidation is linear with time, and if $n = 0.5$, the oxidation progress is parabolic. If n is between 0.5 and 1, intermediate or mixed control oxidation takes place. The oxidation behavior of steel in water vapor at 500–600 °C follows a parabolic oxidation kinetic [1, 35, 36] (Eq. 2).

$$\Delta m = a + b \times t^{0.5} \tag{2}$$

where Δm is the mass change per unit area (mg mm^{-2}), a and b are the regression coefficients for the various materials, t is the oxidation time (min), and $n = 0.5$ in case of parabolic kinetics.

From Fig. 8, all the oxidation kinetics follow a parabolic relationship. For the HSS grade, the initial oxidation is quick at first before a transition to a slower rate. For the semi-HSS grade, after a lower oxidation rate for about 3 min, a sharp increase of rate can be seen for the 15 to 20 following minutes, followed by a slowdown. The semi-HSS grade oxidized at 600 °C shows the highest oxidation rate.

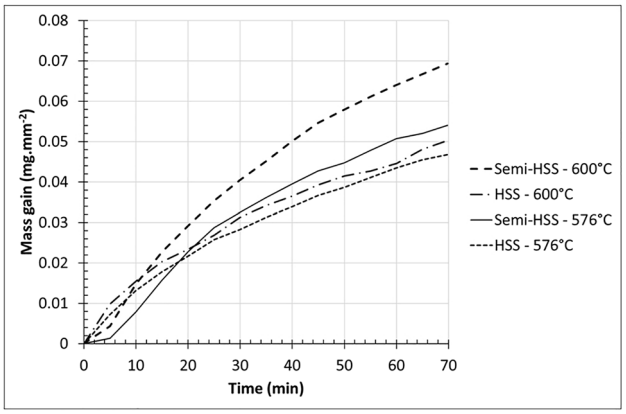

Fig. 8 Oxidation curves (wet atmosphere) of the various samples during oxidation tests at 576 °C and 600 °C

3.7 Sliding wear behavior

The oxide scale formed on the surface of the rolls must be resistant to sliding wear to improve the durability of the surface of the roll. The scale must also adhere to the surface of the roll. The evolution of the friction coefficient with sliding distance for oxidized specimens was studied (Fig. 9). During the sliding wear test (Fig. 9a), for the HSS grade, the mean friction coefficient increases with the increase of the temperature of the oxidation test; for the semi-HSS grade, the friction coefficient remains virtually constant. Moreover, for both grades, after oxidation tests, the friction coefficient is lower than the friction coefficient generally found for steel to steel contact in dry sliding conditions (0.42 from [37]) and remains low after the sliding wear test (Fig. 9b).

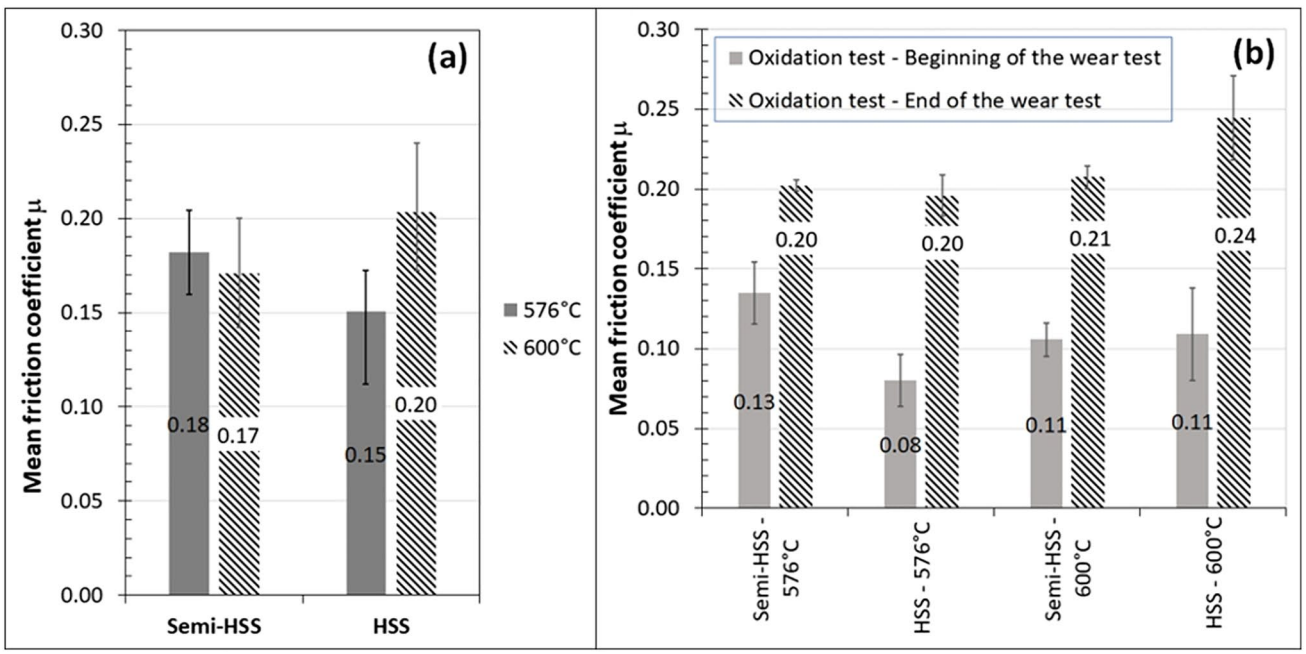

Fig. 9 Oxidized specimens at 576 °C and 600 °C: **a** mean friction coefficient µ during the sliding wear test; **b** comparison of the friction coefficient µ at the beginning and the end of sliding wear test

Table 5 Comparison between the type of carbides found in all grades and the hardness before oxidation tests

Grade	Hardness HV_{30}	Types of carbides
Semi-HSS	686 ± 5	M_2C, MC, (M_7C_3), $M_{23}C_6$
HSS	680 ± 12	M_2C, MC, $M_{23}C_6$

4 Discussion

Table 5 summarizes the links between the type of carbides found in both grades and the hardness before oxidation tests. As expected from [1] and [16], the microstructure of rougher grades (semi-HSS and HSS grades) is composed of a non-continuous network of eutectic carbides located at grain boundaries, embedded in a tempered martensitic matrix (Fig. 2). The presence of M_7C_3 carbides in the semi-HSS grade microstructure, which contain chromium, will provide a high hardness to the shell of the work roll due to the presence of alloying elements such as molybdenum and vanadium (Fig. 3). It was claimed that the low carbon content of semi-HSS grade will provide a very favorable roll bite behavior with a strong increase of hardness and a high wear resistance at low and high temperatures due to the homogeneous matrix.

From [22], it was shown that the formation of secondary phases in the microstructure of steels can affect sliding wear by hardening of the matrix and/or by reducing the real area of contact between a solid body and a counter body. Depending on the identity of phases, the effects can be as follows: changing the tendency for adhesion, changing the fatigue properties or the properties of transfer layers, or giving rise to abrasion.

In the presence of hard MC eutectic carbide in the microstructure of HSS steel, high uneven wear is observed due to the quick worn out of the softer matrix. Moreover, the formation of cell-type MC eutectic with an intercellular network of relatively massive M_2C or M_7C_3 carbides is induced by a large amount of V content. This causes a severe surface irregularity on the roll surface, increasing the interlocking of asperities [15].

The steel grade containing the highest amount of very hard carbides, such as MC-type, presents the highest hardness [1]. The presence of a large amount of very hard MC-type carbides in semi-HSS and HSS grades provides a high hardness (about 685 HV_{30}). As expected from [9], after the oxidation tests, the hardness of the steel substrate decreases. The hardness may be reduced due to thermally induced softening [22]. However, the semi-HSS grade shows a low increase in hardness for the oxidation test at 600 °C compared to 576 °C.

After all oxidation tests, the matrix is homogeneously oxidized. The oxidation progresses inside the steel principally by penetration through the matrix. For all grades studied, the outer oxide layer is not adherent to the surface. Combined with porosity, it would accelerate the wear degradation and increase the friction coefficient.

The XRD analysis of the oxide layers formed on the surface of the sample after oxidation tests shows the formation of four compounds: Fe_2O_3, Fe_3O_4, $FeCr_2O_4$, and CrO (Fig. 1). After oxidation tests, a double-layered oxide forms on the specimen surface, principally composed of Fe_2O_3 (hematite) and Fe_3O_4 (magnetite) [6, 8, 25]. From M. Boccalini Jr. [15], it was found that the oxide layer in HSS rolls consists basically of magnetite, where Cr, Mo, and V are also detected. A spinel $M(Fe,Cr)_3O_4$, produced by the internal oxidation, can also be found [1, 3, 38]. Actually, in the static oxidation test, the humid atmosphere changes the oxidation kinetics, leading to a change in the phase constitution of the surface oxide. The presence of spinel M_3O_4 is known to be beneficial to wear resistance, as well as Fe_3O_4 [9, 38]. In this study, no FeO (wüstite) is detected in any samples. This observation is in accordance with other publications [6, 8, 34, 39]. Moreover, traces of CrO are found. This observation was also made by Zhu et al. [8].

It was shown that the total oxide thickness grows with the temperature of the oxidation tests (Table 2). From Garza-Montes-de-Oca et al. [9], the level of oxidation of the surface of the samples increases with the temperature of the oxidation test, and that the oxide structure does not change dramatically with the temperature of the oxidation test.

For both grades, the mass gain after oxidation tests increases with the temperature of the oxidation test (Table 4). This increase can be linked to the increase in oxide thickness: the lower the mass gain, the lower the scale thickness.

Boccalini [15] has shown that the ideal roll material must be able to develop an oxide layer that rapidly forms and regenerates, but, once formed, slowly grows to keep a high adherence to the roll surface. For HSS grade, the initial oxidation rate is quick before a transition to a slower rate. The high-temperature oxidation rate can be divided into three stages: parabolic, linear, and intermediate. Due to the increase of the oxide scale thickness and to the formation of a thick compact structure of hematite at the top of the scale, after a linear initial stage controlled by the diffusion rate of the oxygen atoms, the process of oxidation becomes parabolic and the oxidation rate becomes slower [36, 40]. Moreover, whatever the temperature of the oxidation test, the oxidation behavior of both grades follows a parabolic oxidation kinetic (Fig. 8). Those results confirm the observation made by Kim et al. [6] for HSS steels oxidized at 600 °C in a wet atmosphere. The semi-HSS grade shows the highest oxidation rate at 600 °C. This can be linked to the progression of the oxidation inside the steel: the presence of many cracks in the scale accelerates the surface oxidation of

the steel [6]. As the scale is more porous after oxidation at 600 °C, the oxidation rate is higher.

As expected from [6], the oxide layer developed on the steel surface presents a double structure: an outer layer with a columnar and porous structure, and an inner one with a fine and dense microstructure (Figs. 2 and 6). As the outer layer contains many cracks and defects, the oxygen- and Fe-ion diffusion is accelerated, producing a thick scale. The inner layer being more compact, it can act as a protective layer reducing further oxidation [2].

In Hot Strip Mill, the surface roughness of the work roll must be high to prevent slipping. The scale must also provide a high friction coefficient to increase the wear resistance of the roll. The surface roughness R_a is lowest for the HSS grade whatever the temperature of the oxidation test, and highest for semi-HSS grade oxidized at 600 °C (Table 3). However, the effect of the initial surface finish (initial roughness) on friction and wear is limited to the running-in period, depending on the degree of change of surface quality during the sliding contact. This is strongly dependent on the material properties and loading conditions. Not only the roughness but also the asperity curvature on surfaces influences the wear. Rounded asperities on a harder counterface promote wear by surface fatigue, while sharp asperities favor wearing by micro-cutting [22].

It is generally admitted that the friction coefficient increases with the temperature of the oxidation test [9]. Figure 9 a shows that this is the case for the HSS grades. For the semi-HSS grade, the friction coefficient remains constant whatever the temperature of the oxidation test. The formation of oxides on the surface of the rolls subject to sliding reduces the friction coefficient [26] because the oxide is harder than the substrate and it may act as a solid lubricant if this oxide is smooth adherent, and continuous [15]. Belzunce et al. [1] have shown that a higher friction coefficient is found for HSS steels showing a higher oxidation rate due to the selective oxidation of certain carbides such as MC-type. In this study, an increase in friction coefficient for the HSS grade can be linked to an increase in mass gain for the oxidation test from 576 to 600 °C. Moreover, the friction coefficient increases during sliding wear tests (Fig. 9b). This is due to the formation of wear particles or debris when two surfaces are sliding in contact. Some of those debris remain in contact and can be retransformed by further sliding [41]. The extra energy spent to drag the debris from the contact increases the friction coefficient and the wear due to the abrasive nature of hard oxidized particles [42].

The links between the evolution of the friction coefficient and the hardness are not obvious because different wear mechanisms can be encountered, depending on the operating conditions [22]. For this reason, the wear intensity may decrease, increase, or be unaffected by the hardness of the materials in contact. However, the lowest abrasion wear rates are found for steel containing a higher MC content. As the hardness is linked to the hard MC-type carbide content, steel with a high hardness will provide a low abrasion wear rate.

5 Conclusions

The oxidation behavior at 576 °C and 600 °C in a wet atmosphere of two grades of ferrous alloys (semi-HSS and HSS grades) that could be used in hot rolling mills was analyzed. The following conclusions were reached:

- After oxidation tests, a double-layered oxide is found on the specimen surface, principally composed of Fe_2O_3 and Fe_3O_4, with the presence of a spinel $FeCr_2O_4$ localized in the inner oxide layer and some traces of CrO. No FeO is detected. This double structure is composed of an outer layer with a porous structure, and an inner one with a fine and dense microstructure. Cracks are found through the entire scale and reach the unoxidized matrix, accelerating the oxidation process.
- The oxidation progresses inside the steel principally by penetration through the tempered martensite matrix. For the HSS grade, the oxidation progresses through M_2C carbides and MC-type are unaffected.
- The oxidation process is parabolic for all grades, which suggests that the diffusion of metal cations or oxygen anions is the rate-controlling step.
- The surface roughness R_a is lowest for the HSS grade whatever the temperature of the oxidation test, and highest for the semi-HSS grade oxidized at 600 °C. For both grades, R_a is high enough (2.5 to 4.6 µm) to prevent slipping.
- The low friction coefficient found for both grades (0.2) after oxidation tests will increase the wear resistance of the roll.
- After oxidation tests, the hardness decreases but remains higher enough to ensure wear resistance (from about 680 HV_{30} to about 500–570 HV_{30}, before and after oxidation tests, respectively).
- Considering the above results, both grades can be used in the roughing stand or the F1 finishing stand of hot rolling mills.

Acknowledgements The authors wish to thank Materia Nova (Mons, Belgium) for the SEM analysis and the Laboratory of Physics of Surfaces and Interfaces of UMONS (Mons, Belgium) for the tribotests.

Author contribution All authors contributed to the study conception and design. Material preparation, data collection, and analysis were performed by Fabienne Delaunois, Victor Ioan Stanciu, Alexandre Mégret, and Mario Sinnaeve. The first draft of the manuscript was written by Delaunois Fabienne, and all authors commented on previous

versions of the manuscript. All authors read and approved the final manuscript.

Funding This work was supported by the Région Wallonne, Belgium (grant number 7522).

Data availability All data and materials support our published claims and comply with field standards.

Code availability Not applicable.

Declarations

Ethics approval Not applicable.

Consent to participate Not applicable.

Consent for publication Not applicable.

Conflict of interest The authors declare no competing interests.

References

1. Belzunce FJ, Ziadi A, Rodriguez C (2004) Structural integrity of hot strip mill rolling rolls. Eng Fail Anal 11(5):789–797. https://doi.org/10.1016/j.engfailanal.2003.10.004
2. Joos O, Boher C, Vergne C, Gaspard C, Nylen T, Rezaï-Aria F (2007) Assessment of oxide scales influence on wear damage of HSM work rolls. Wear 263(1–6 SPECS. ISS):198–206. https://doi.org/10.1016/j.wear.2007.02.005
3. Molinari A, Pellizzari M, Biggi A, Corbo G, Tremea A (2002) Primary carbides in spincast HSS for Hot Rolls and their effect on the oxidation behaviour. 6th Int Tool Conf Karlstad S 365–377
4. Deng GY et al (2017) Theoretical and experimental investigation of thermal and oxidation behaviours of a high speed steel work roll during hot rolling. Int J Mech Sci 131–132:811–826. https://doi.org/10.1016/j.ijmecsci.2017.08.024
5. Lecomte-Beckers J, Breyer J (2004) Structural investigations of HSS rolls for hot strip mill. Proc. 41st Roll. Semin., no. ABM, pp. 89–98
6. Kim HH, Lim JW, Lee JJ (2003) Oxidation behavior of high-speed steels in dry and wet atmospheres. ISIJ Int 43(12):1983–1988. https://doi.org/10.2355/isijinternational.43.1983
7. Hao L et al (2015) High temperature oxidation investigation of hot roll material with high-speed steel. Adv Mater Res 1095:130–134. https://doi.org/10.4028/www.scientific.net/amr.1095.130
8. Zhu Q, Zhu HT, Tieu AK, Kong C (2011) Three dimensional microstructure study of oxide scale formed on a high-speed steel by means of SEM, FIB and TEM. Corros Sci 53(11):3603–3611. https://doi.org/10.1016/j.corsci.2011.07.004
9. Garza-Montes-de-Oca NF, Rainforth WM (2009) Wear mechanisms experienced by a work roll grade high speed steel under different environmental conditions. Wear 267(1–4):441–448. https://doi.org/10.1016/j.wear.2009.01.048
10. Vitry V, Nardone S, Breyer JP, Sinnaeve M, Delaunois F (2012) Microstructure of two centrifugal cast high speed steels for hot strip mills applications. Mater Des 34:372–378. https://doi.org/10.1016/j.matdes.2011.07.041
11. Pellizzari M, Cescato D, De Flora MG (2009) Hot friction and wear behaviour of high speed steel and high chromium iron for rolls. Wear 267(1–4):467–475. https://doi.org/10.1016/j.wear.2009.01.049
12. Delaunois F, Stanciu VI, Sinnaeve M (2018) Resistance to high-temperature oxidation and wear of various ferrous alloys used in rolling mills. Metall Mater Trans A Phys Metall Mater Sci 49(3):822–835. https://doi.org/10.1007/s11661-017-4450-x
13. De Colnet L et al (2001) Quantitative description of MC, M2C, M6C and M7C3 carbides in high speed steel rolls. Proc MSMF-3 Int Conf held Brno, pp 710–717
14. Lecomte-Beckers J, Mario S, Jerome TT (2011) New trends in hot strip mill roughing mills: characterization of high chromium steel and semi-HSS grades. AISTech - Iron Steel Technol. Conf. Proc., no. October, pp. 1771–1782
15. Boccalini M Jr, Sinatora A (2002) Microstructure and wear resistance of high speed steels for rolling mill rolls. 6th Int Tool Conf, pp. 509–524
16. Lecomte-beckers J, Sinnaeve M, Tchoufang Tchuindjang J (2012) Current developments of alloys steels for hot strip roughning mills: characterization of high-chromium steel dans semi-high speed steel. pp. 33–40
17. Lecomte-beckers J, Sinnaeve M, Tchoufang Tchuindjang J (2010) Comparison between HCS and semi-HSS grades used as work rolls in the roughing stand of Hot Strip Mills. Proc. 10th Int. Conf. Steel Roll., no. March 2015
18. Jacqueline LB, Mario S, Jerome TT (2011) New trends in Hot Strip Mill roughing mills: characterization of high chromium steel and semi-HSS grades, AISTech - Iron Steel Technol. Conf Proc I:1771–1782
19. Hutchings I, Gee M, Erich S (2006) Friction and wear. In: Smith H, Czichos T, Saito L (eds) Springer handbook of materials measurement methods. Springer, Berlin, Heidelberg, pp 685–710
20. Stachowiak GW, Batchelor AW (2006) Abrasive, erosive and cavitation wear. In: Stachowiak GW, Batchelor AW (eds). Engineering Tribology, pp 501–551
21. Gaona-Martínez MJ et al (2019) Effect of tempering on the oxidation behaviour of a roll-grade high-speed steel during thermal cycling. Oxid Met 91(5–6):641–656. https://doi.org/10.1007/s11085-019-09900-6
22. Karl-Heinz ZG (ed) (1987) Sliding wear. In: Microstructure and Wear of Materials, pp. 351–495
23. Spuzic S, Strafford KN, Subramanian C, Savage G (1994) Wear of hot rolling mill rolls: an overview. Wear 176(2):261–271. https://doi.org/10.1016/0043-1648(94)90155-4
24. Vergne C, Boher C, Gras R, Levaillant C (2006) Influence of oxides on friction in hot rolling: experimental investigations and tribological modelling. Wear 260(9–10):957–975. https://doi.org/10.1016/j.wear.2005.06.005
25. Magnee A, Gaspard C, Coutsouradis D (1977) Analyse De Sollicitations De Cylindres De Travail a Chaud. Rev Metall Cah D'Informations Tech 74(1):35–52. https://doi.org/10.1051/metal/197774010035
26. Stott FH (1998) The role of oxidation in the wear of alloys. Tribol Int 31(1–3):61–71. https://doi.org/10.1016/S0301-679X(98)00008-5
27. Rizzo FC, Monteiro MJ, Saunders SRJ (2009) Effect of alloying additions on the oxidation of high speed steels under dry and wet conditions. J Chin Soc Corros Prot 29(4):241–247
28. Young DJ (2016) Alloy oxidation II: internal oxidation. In High Temperature Oxidation and Corrosion of Metals, John Fedor, pp. 261–333
29. Hao L, Li T, Xie Z, Duan Q, Zhang G (2020) The oxidation behaviors of indefinite chill roll and high speed steel materials. Metals (Basel) 10(8):1–10. https://doi.org/10.3390/met10081095
30. Deng GY et al (2017) Evolution of microstructure, temperature and stress in a high speed steel work roll during hot rolling: experiment and modelling. J Mater Process Technol 240:200–208. https://doi.org/10.1016/j.jmatprotec.2016.09.025

31. Serajzadeh S (2008) Effects of rolling parameters on work-roll temperature distribution in the hot rolling of steels. Int J Adv Manuf Technol 35(9–10):859–866. https://doi.org/10.1007/s00170-006-0764-3
32. Weidlich F, Braga APV, da Silva Lima LGDB, Júnior MB, Souza RM (2019) The influence of rolling mill process parameters on roll thermal fatigue. Int J Adv Manuf Technol 102(5–8):2159–2171. https://doi.org/10.1007/s00170-019-03293-1
33 Chang YN (1989) Wei FI (1989) High temperature oxidation of low alloy steels. J Mater Sci 24(1):14–22. https://doi.org/10.1007/BF00660927
34. González V, Rodríguez P, Haduck Z, Colás R (2001) Modelling oxidation of hot rolling work rolls. Ironmak Steelmak 28(6):470–473. https://doi.org/10.1179/irs.2001.28.6.470
35. Ramírez-Ramírez JH, Colas R, Garza-Montes-de-Oca NF (2013) High temperature oxidation of a work roll grade high-chromium white cast iron. J Iron Steel Res Int 20(10):122–129. https://doi.org/10.1016/S1006-706X(13)60187-9
36. Garza-Montes-De-Oca NF, Colás R, Rainforth WM (2011) High temperature oxidation of a work roll grade high speed steel. Oxid Met 76(5–6):451–468. https://doi.org/10.1007/s11085-011-9266-2
37. Fuller DD (1956) Coefficients of friction. In: Theory and Practice of Lubrication for Engineers, pp. 42–48
38. Sullivan JL, Athwal SS (1983) Mild wear of a low alloy steel at temperatures up to 500°C. Tribol Int 16(3):123–131. https://doi.org/10.1016/0301-679X(83)90053-1
39. Zhu Q, Zhu HT, Tieu AK, Reid M, Zhang LC (2010) In-situ investigation of oxidation behaviour in high-speed steel roll material under dry and humid atmospheres. Corros Sci 52(8):2707–2715. https://doi.org/10.1016/j.corsci.2010.04.027
40. Tuck CW, Odgers M, Sachs K (1969) The oxidation of iron at 950°C in oxygen/water vapour mixtures. Corros Sci 9(4). https://doi.org/10.1016/s0010-938x(69)80056-9
41. Fischer TE, Zhu Z, Kim H, Shin DS (2000) Genesis and role of wear debris in sliding wear of ceramics. Wear 245(1–2):53–60. https://doi.org/10.1016/S0043-1648(00)00465-8
42. Yuan CQ, Peng Z, Zhou XC, Yan XP (2005) The characterization of wear transitions in sliding wear process contaminated with silica and iron powder. Tribol Int 38(2):129–143. https://doi.org/10.1016/j.triboint.2004.06.007